Geotechnical properties of uncompacted DNA-1A lunar simulant

GEOTECHNICAL PROPERTIES OF UNCOMPACTED DNA-1A LUNAR SIMULANT

V. Marzulli (*), F. Cafaro (**)

(*) Valentina Marzulli, PhD student

Friedrich-Alexander Universität Erlangen-Nürnberg, Institute for Multiscale Simulation

Nägelsbachstrasse 49b, 91052 Erlangen (Germany)

e-mail: valentina.marzulli@fau.de

(**) Francesco Cafaro, Assistant Professor

DICATECh – Technical University of Bari, Bari (Italy)

Via Orabona 4, 70125 Bari (Italy)

e-mail: francesco.cafaro@poliba.it (corresponding author)

Accepted by Journal of Aerospace Engineering (ASCE) - DOI number: 10.1061/(ASCE)AS.1943-5525.0000983 (in print)

ABSTRACT

Understanding the mechanical behaviour of lunar regolith is of great importance to address the building of structures on the Moon, as well as for predicting the response of some equipments or facilities interacting with the lunar soil (i.e. rovers). Since the amount of lunar regolith samples on Earth is quite low due to the difficulties to bring it back during space missions, in the last decades researchers started to develop similar materials, usually named lunar regolith simulants. This paper reports the geotechnical characterization of DNA "De NoArtri" lunar simulant carried out in the laboratory. Compositional analyses and mechanical tests have been carried out to characterize this simulant: particle-size distribution analysis, chemical analysis, scanning electron microscope (SEM) analysis have been performed, to identify the DNA-1A from a compositional point of view, as well as triaxial compression tests, direct shear tests and oedometer tests for depicting its mechanical behaviour, with some comparison with the original lunar soil and other simulants.

KEYWORDS

lunar simulant; lunar soil; DNA simulant; Moon; loose behaviour; lunar structures.

INTRODUCTION

In recent years, attention is increasingly being focused on the building of structures on the Moon. It represents a crucial challenge for the future of mankind and for this reason several research groups involved in this field are gearing their efforts to obtain practical results in a few years. In this context, the main space agencies in the world are developing programmes for realizing a permanent moonbase: for example the European Space Agency's (ESA) Moon Village vision can be mentioned, which involves the planning of a lunar settlement in a perspective of international collaboration.

In general, designing geotechnical structures require a deeper understanding of the way in which the structures interact with soil, therefore modelling the soil-structure interaction in lunar environment requires accurate definition of the mechanical behaviour of the lunar regolith. Furthermore, it is of great importance to figure out how to model the above-mentioned soil-structure interaction at a terrestrial gravity level for predicting the corresponding behaviour on the Moon, since in this case it is not possible to construct a full-size prototype but the model of the geotechnical system must be scaled for the gravity acceleration (Cafaro et al., 2018). In this respect, centrifugal experiments with simulated regolith have been performed (Omura et al. 2016).

In the last decades, space missions have led to get important data about the characteristics of lunar surface and lunar soil, as well as to collect small amounts of regolith. This has allowed to characterize its composition, its geotechnical properties and hence to define the most important mechanical parameters (Carrier 1973; Carrier et al. 1973). Nevertheless, performing tests on the Earth to predict the behaviour of a lunar structure requires using a large quantities of material. It has triggered to carry out research into alternative materials, defined as simulant.

In this respect, the simulant mechanical parameters of engineering value should concern both strength and deformability characteristics. Indeed, the performance of a lunar geotechnical structure must be assessed not only looking at the collapse but also in terms of serviceability, that is looking at small strains scenarios. Consistently, the soil shear stiffness should be measured at small to medium strain levels. Moreover, the mechanical parameters should mainly refer to low confining pressures, as resulting in a low gravity environment.

Several simulants have been created over the years: although they have roughly the same characteristics, each of them has peculiar features which should guide the engineers in the choice of the material to be used for experimental tests, depending on the specific aspect of the design. For instance, the Minnesota Lunar simulant (MLS-1), the first to be created, is totally crystalline and has been created to approximate the composition of Apollo 11 lunar soil samples (McKay et al., 1994). One of the first and most studied lunar regolith simulants is probably the Johnson Space Center simulant (JSC-1) and its following versions (JSC-1A, JSC-1AF, JSC-1AC). JSC-1 is a basaltic ash which possesses huge amount of glass. It has been created to approximate the properties of a low-titanium mare soil found at the Apollo 14 site and to complement the MLS-1 (McKay et al., 1994, Willman et al., 1995, Pitcher et al., 2016). The reason why this lunar simulant is widely characterized also lies in its use for manufacturing lunarcrete (Markandeja Raju and Pranathi, 2012). To approximate the properties of the regolith characterizing the lunar polar region, the NASA/USGS Lunar Highlands Type simulants (NU-LHT) have been developed. These simulants have the same particle-size distribution as the JSC-1A but different mineralogy. While NU-LHT simulants are composed of a mixture of glass, agglutinates and plagioclase, JSC-1A is composed of lithic fragments (Schrader et al., 2010; Pitcher et al., 2016). The Glenn Research Center simulant (GRC-3) has been created to allow the study of geotechnical problems, like excavation ad wheel-soil interaction (Suescun-Florez et al. 2014), while the DNA simulant has been recently involved in the ESA research project for manufacturing lunarcrete by using the 3D printing technology (Cesaretti et al., 2014). Meurisse et al. (2017) carried out a study on the influence of mineral composition on sintering lunar regolith, in which the DNA is compared with other simulants (i.e.: FJS-1 and JSC-1a).

Due to the growing attention for the DNA-simulant, its geotechnical characterization becomes important, to allow a correct modelling of the interaction between cohesionless regolith (soil) and sinterized regolith (structure). In this study, the geotechnical properties and the mechanical behaviour of the cohesionless DNA simulant are shown and discussed. In particular, the material has been studied fundamentally in loose (uncompacted) state, since this condition should be plausibly the “operational” one for the soil when placed by the rovers on the Moon to fastly realize a cover protecting the first habitat from micrometeoroids and solar radiations. In this work, it will be proposed to name the tested material as DNA-1A, to distinguish it from the DNA-1 samples used by Cesaretti et al. (2014) in their research, which partially differ in terms of chemical composition due to some variability characterizing the soil in the quarry.

In the following section, the composition of the studied lunar simulant is presented, both from a chemical and a mineralogical point of view, together with the grain size distribution and the particle morphology. Then, after describing the testing procedures adopted in the experimental campaign, the results obtained by the tests carried out in the laboratory are presented and discussed, also on the basis of comparison with the features of other simulants mentioned in the literature. Finally, in the concluding section, it is pointed out how to address future work, both numerical and experimental, implementing the results of the present characterization in numerical simulations of physical model behaviour concerning lunar structures.

COMPOSITION OF LUNAR SIMULANT DNA-1A

The studied material (Figure 1) has the same origin as the DNA-1 simulant (Cesaretti et al. 2014). The ash was mined from a commercial cinder quarry at Onano (north flank of Bolsena Crater, Italy). Following coarse sieving, the ash was crunched in an impact mill. Ashes from several millings were allowed to partially dry in air and then mixed. The mix was further grinded and then passed through a 0.125 UNI2332 sieve. The average water content of the final mix was 1.7% in weight. However, due to further loss of humidity with time, the water content of the specimens employed in the testing programme has resulted much lower than this value, even 0.8%, that should be considered as a hygroscopic content.

The specific gravity, G_s, of DNA-1A has been measured by using 100 ml water picnometer. A value of G_s of 2.70 has been found, as a mean of two measures: this value is lower than that found by Cesaretti et al. (2014) for DNA-1, equal to 2.91 and more consistent with the range reported by Carrier et al. 1991 for the lunar soil density, which fluctuates between 2.90 and 3.10. However, some other simulants are characterized by lower G_s values: the BP-1 has specific gravity equal to 2.81 (Suescun-Florez et al. 2014) and the GRC-3 is characterized by a value of 2.63 (He et al. 2013).

Particle-size distribution

Since segregation during transportation may appear, two different samples of DNA-1A lunar simulant have been taken from two different depths within the package to carry out granulometry analyses. The samples are labelled in the figures as Sample 1 and Sample 2. Two methodologies have been associated: 1) ASTM sieve

analyses for the coarser fraction (particle diameters greater than 0.125 mm); 2) Beckman Coulter Multisizer 4 counter for the finer fraction. The resulting particle-size distribution is shown in Figure 2a.

It can be noticed that the sorting of the two samples can be considered to be quite similar: the uniformity coefficient, defined as the ratio D_{60}/D_{10}, is 4.8-5.2. In Figure 2b the particle-size distributions of the most studied lunar simulants are also reported. The granulometry is fundamentally the same for all the materials, as expected, since the simulants are artificial soils created by mixing known amounts of the different fractions, in order to reproduce the lunar soil granulometry. However, some differences in sorting are possible (and expected also on the Moon) and can result in different soil porosity for a given compaction level. Suescun-Florez et al. (2014) found a uniformity coefficient for BP-1 equal to 10.47, Perkins and Madson (1996) mention a value of 16 for MLS-1, the same value reported by Carrier (2003) for the lunar regolith, and He et al. (2013) reported a value of 10 for GRC-3. Therefore, compared to these values, the sorting of DNA-1A is relatively low, making it more prone to reach loose states under self-weight compaction.

Mineralogy and chemical composition

Cesaretti et al. (2014) reported the major crystalline phases of DNA-1, listed in order of abundance:

- Analcime (Feldspatoid mineral) Plagioclase (Feldspar mineral)
- Pyroxene (Diopside)
- Mica (Phologopite)
- Traces of Calcite
- Traces of Quartz (Silicon dioxide)

No Olivine has been found. According to Meurisse et al. (2017), the glass in the DNA simulant is absent and the grains are fully crystallized. Previous studies showed that the JSC-1A glass phase comprises 27–49 vol.% (Hill et al. 2007; Schrader et al. 2008). The average glass content measured on samples from the Apollo missions 11 to 16 varies in the range 6.6-29.4 (Markandeja Raju and Pranathi, 2012). Glass beads on the Moon are volcanic beads, or shock-melt, generated by micrometeorite impacts, which has quenched in flight (Liu et al. 2008). In this respect, every lunar simulant could be enriched in terms of glass content by addition of a suitable fraction, depending of the aim of the experimental study (i.e. sintering, mechanical tests), although the

high variability of the glass content in the lunar soils makes questionable the choice of the amount of glass to be added to the simulant.

The chemical composition of the tested DNA-1A samples has been identified using the X-ray fluorescence analysis for two samples of lunar simulant. Chemical tests have been carried out using Panalytical AXIOS-Advanced spectrometer. The results are shown in Figure 3.

The difference between the two samples is negligible. A comparison between DNA-1A and other simulants, as well as with the original lunar soil, is summarized in Table 1, where the chemical composition of DNA-1, JSC-1A and Lunar Soil 14163 (mean of the Apollo missions) are reported (Cesaretti et al. 2014; Rickman et al. 2007), together with the average of the two DNA-1A samples.

As expected, some chemical variability can be detected from the table. In particular, with respect to JSC-1A and to DNA-1, the simulant, DNA-1A has SiO_2 markedly higher: the value pertaining Lunar Soil 14163 is in between their values. High content in SiO_2 has been found also for the Korea Lunar Simulant, KLS-1, 48% (Ryu et al. 2018), and for MKS-1 from Japan, almost 53% (Kanamori et al. 1998). TiO_2 is lower for DNA-1A, making this simulant able to mimic low-Ti mare soil (Meurisse et al. 2017), whereas Al_2O_3 is consistent with the mean from Apollo missions. Relatively low is the content in ferric oxide, Fe_2O_3 (about 7%) for DNA-1A: in this respect, it should be considered that the absence of atmosphere on the Moon involves no oxidation, the reason why the lunar soils, formed in a reducing environment, have iron in the form of Fe_2 and FeO (Markandeya Raju and Pranathi, 2012). Rickman et al. (2007) reported a very low value for Fe_2O_3 in JSC-1A (3.41%), whereas for the simulant BP-1 Suescun-Florez et al. (2014) reported a value of about 6% (Stoeser et al. 2010). Some differences among the materials in Table 1 can be detected also for other oxides. The difference in terms of SiO_2 and Fe_2O_3 between DNA-1 and DNA-1A could justify their difference in specific gravity.

SEM analysis

Given the effects of particle shape on porosity (Omura et al., 2016) and on the friction between particles, it is important to provide information concerning the grain morphology of a soil. SEM analyses have been carried out on DNA-1A lunar simulant to point out the recurrent particle morphology and to make some comparisons with the original lunar soils. From each sample, through wet sieving, particles of diameter in between 0.125 mm and 0.090 mm, have been selected. This amount of material has been cleaned by ultrasonic bath with

distilled water for about 10 minutes and then dried in oven at 70 °C for 24 hours. The technique followed to obtain microscopy images is called backscattered electrons (BSE). Only particles of diameter in the range of 0.090 mm to 0.125 mm have been analysed, since this range seems to be the most representative of the fragmentation processes related to the formation of the material.

SEM images are shown in Figure 4 at different magnification (75x, 400x, 750x, 850x, 1100x, 1200x).

In Figure 4a, a general view of this volcanic ash can be observed. Two main grain textural types have been recognized:

- clast with vesicles of irregular shape generated by the presence of magma (Fig. 4b-c-d);
- fragments of juvenile material rich in crystal and minerals (Fig. 4b-e-f), sometimes with small particles attached to each other.

A study in terms of texture and shape of the particles of the lunar dust can be found in Liu et al. (2008). According to the authors, based on both their SEM observations and the literature, the lunar dust grains can be classified into five types: glass beads, vesicular texture, angular shards, blocky fragments, aggregated particles (normally on uncleaned samples). However, it is difficult to find identical textural features in a terrestrial soil. An important difference between lunar regolith and its simulants is for example the interparticle adhesion present in lunar regolith (Costes and Mitchell 1970; Suescun-Florez et al. 2014), which could be explained in terms of different specific surface of the particles, in turn arising from the different environment. Indeed, the absence of erosion processes on the Moon implies the persistence of high angularity and roughness for the soil particles.

GEOTECHNICAL PROPERTIES OF DNA-1A

Soil density and testing procedures

Mechanical tests have been carried out on DNA-1A specimens in dry conditions (except for one test), which can be considered to be of major interest for a geotechnical lunar structure and given the incidence of the water on the mechanical behaviour of the soils, as for the compressibility of sands (Wils et al. 2015). The above-mentioned tests have been aimed at determining both the soil compressibility parameters and the shear strength parameters. All the tests have concerned self-weight compacted specimens.

Minimum and maximum soil densities have been determined according to the following procedures. For the minimum density measurement, 196.6 g of soil have been dropped from the top of a rigid transparent cylinder of 42 cm inner diameter and 20 cm height, by interposing a 10 ASTM sieve, on which the material has been spread and passed through the mesh, in order to make the sedimentation in the cylinder as uniform as possible. The resulting volume has allowed to calculate the corresponding dry density. However, since this value has resulted to be higher than the lowest density among those measured on all the specimens realized during the testing programme, which was 0.98 g/cm^3, this last value has been selected as minimum density of the material (Table 2). The same cylinder, filled with loose DNA-1A for almost 10 cm, has been placed on a shaker (G.G.T. shaker), in order to determine the maximum dry density. First, vibrations have been applied to the column for 5 minutes at the lowest velocity of the machine. Thereafter, a cylindrical steel top of 686 g, with horizontal section slightly smaller than the column, has been put on the soil and vibrations have been applied for further 5 minutes. The maximum density (Table 2) has been then calculated using the final volume occupied by the material, of known weight, after leveling the soil at the same height by beating it. The values in Table 2 seem to be consistent with the corresponding values of lunar soil 14163 (Carrier et al. 1973; Carrier 1973). On the basis of these values, the relative density of the specimens created for the direct shear tests is about 20%, while for the specimens created for the triaxial tests is on average 70%. This discrepancy could be explained considering that the porosity of the specimens, according to the procedure followed for their creation and described below, results from self-weight compaction and, therefore, the difference in height between triaxial and shear box specimens should imply different relative densities.

Four oedometer tests have been performed on loose specimens. In particular, two tests have been carried out on the same specimen, of 56 mm diameter and 20 mm height, which has been first subjected to loading up to 5 MPa vertical stress, in dry condition (MP5), then unloaded and, after prolonged submersion, reloaded up to 5 MPa again (MPW). The other two one-dimensional compressions (HP5 and HP15), concerning specimens in dry condition of 50 mm diameter and 20 mm height, have been carried out up to 18 MPa vertical stress, by using an apparatus with three arms (Figure 5), in order to better detect the gross-yield pressure range of the soil. The readings of the specimen settlement at each loading step have been taken after 5 minutes for all the tests, expect on HP15 (readings taken after 15 minutes), assuming no primary consolidation. The specimen settlements measured during the tests have then been corrected for the compliances of the apparatus, in turn

measured using a steel specimen. The last load step of the high pressure test HP15 has been prolonged for about 8 months with the aim of monitoring the soil creep and, after this period of time, the specimen has been subjected to a wetting collapse test.

Eight consolidated drained (CD) triaxial compression tests have been carried out at confining pressure of about 20 KPa, 40 KPa, 60 KPa, 100 KPa and 150 KPa, on dry specimens of about 38 mm diameter with an approximately 2:1 length to diameter ratio. Four tests (set A), namely A-TRX-100kPa A-TRX-60kPa A-TRX-40kPa A-TRX-20kPa, have been performed using a rigid membrane of about 1 mm thickness, which once placed on the pedestal is able to maintain a quasi-cylindrical shape when filled with soil (Figure 6a), while the other four tests (set B), namely B-TRX-150kPa B-TRX-100kPa B-TRX-60kPa B-TRX-40kPa, have been carried out using a thinner membrane and a split mould (Figure 6b), in order to check the repeatability of the results by using membranes with different stiffness. Specimens have been made using a teaspoon for filling the space surrounded by the membrane. The initial porosity of each specimen has been calculated "a posteriori" on the basis of the measurements of the specimen diameter at different heights and of the amount of soil mass employed. A mean bulk density value of 1.33 g/cm^3, with standard deviation of 0.07 g/cm^3, has been found.

During the tests, air flushing through the pedestal has been allowed (i.e. "drained conditions") and between the specimen and the pedestal a dry porous stone, interposed between two filter paper disks, has been placed. The filters were aimed at preventing clogging of the porous stone and of the air drainage circuit. The triaxial compression tests have been strain-controlled with rate of displacement of 0.0019 mm/min. This relatively low rate has been chosen to prevent air from getting trapped in the pores during compression. Moreover, during two tests (A-TRX-40kPa and A-TRX-20kPa) local axial displacements have been measured by local strain gauge RDP series D5/200WRA, mounted with glou on the thick membrane (Figure 6c).

Using triaxial tests the material shear behaviour has been observed on a huge range of confining pressures, but it was difficult to carry out tests at very low radial stress. Therefore, direct shear tests have been performed with the aim of deducing strength parameters at lower confining pressures (3.4, 5.5, 7.5, 9.5, 10.2, 15, 19.8 and 60 kPa). These tests have been also aimed at detecting the pressure range of transition from dilative to contractive shear behaviour. The specimens placed in the shear box were square with 6 cm side and 2 cm height. The horizontal displacement rate has been imposed to be equal to 0.05 mm/min for all the direct shear tests.

Compression Behaviour

1D compression

In Figure 7 the one-dimensional compression curves obtained in the oedometer tests on the uncompacted simulant are shown. As described in the testing procedure, one of them (MPW) concerns the same specimen of the test MP5 after being submerged. Its compression curve lies to the left of the "dry" ones. All the curves of the dry specimens are consistent between them, with some discrepancy in terms of initial porosity. The yield vertical stress seems to be more evident during the high pressure tests. Indeed, using the pressure range of the conventional tests, it is difficult to reach the Normal Compression Line, NCL (Schofield and Wroth, 1968), of a sand, due to its relatively high stiffness compared to other soils such as clays or silts. Although based on the position of the compression curve MP5 (Figure 7) one could suspect that the NCL has not been reached, from the curves corresponding to the high pressure tests (HP15 and HP5) a gross-yield (Hight et al., 1992; Cotecchia and Chandler 2000) vertical effective stress, σ'_y, of about 800-900 kPa can be estimated. This value, relatively low for a sandy soil, arises from the loose states of the specimens, which lie near the NCL at high specific volumes and low pressures, according to the Critical State soil mechanics framework for sands (Atkinson and Bransby 1978; Wood 1990): it is expected that after densification the gross-yield of this soil will be much greater.

In terms of compressibility (Table 3), before the yield stress range the dry material exhibits a recompression index of 0.061 to 0.104, slightly higher than the corresponding parameter for the wet sand. Beyond the yield stress the compression index of the dry material seems to reach a value of 0.224 to 0.333. During unloading (MP5 test) a swelling index of 0.013 has been measured, showing a very limited swelling ability of this material. The compressibility of lunar soils reported by Leonovich et al. (1974, 1975) and Gromov et al. (1972) is characterized by values which confirm that the DNA-1A simulant can be used to reproduce the compression behaviour of the same lunar soils.

Creep behaviour

Due to the presence of vesicular grains in the volcanic ashes, as detected by SEM for DNA-1A (Figure 4), it is plausible that under prolonged and higher stresses these grains undergo crushing, since it is expected that the vesicular texture makes a particle prone to crush when the contact forces are high.

The creep behaviour of DNA-1A has been monitored during the last loading step of the high pressure oedometer test, at a vertical effective stress of about 18 MPa. The void ratio is plotted versus time in Figure 8: from the curve few phenomena of increase of compressibility can be recognized, probably due to the occurrence of sudden soil crushing: the secondary consolidation coefficient $C_\alpha = \Delta e/\Delta \mathrm{Log}(t)$, calculated over the entire period of about 8 months, fluctuates around 0.004.

This information should be useful particularly when dealing with long term serviceability assessment for a lunar geotechnical structure. Although in the present study attention has been paid to the creep behaviour at high confining pressures, which could reveal peculiar features of the microstructural damage evolution, the geotechnical design for Moon should be based on creep measurements at low confining pressures. Therefore, further experimental research is needed to observe the creep behaviour of the material under very low stresses and very long duration.

Wetting collapse

The collapse under wetting is a typical phenomenon characterizing the sandy soils, particularly in dry condition, and it can cause important settlements of geotechnical works. A wetting test has concerned the specimen previously subjected to high pressure oedometer compression and creep monitoring, at a void ratio of about 0.73 and under vertical stress of about 18 MPa. The specimen has been fully submerged and the measurement has been taken at 24 hours: volumetric strain of 2.20% has been measured. Although this condition should not characterize the real lunar soils interacting with the future moonbase, similar occurrence could involve the same soil if covered under pressurized environment and subjected to imbibition for human activities.

Shear behaviour

Shear strength

In Figure 9, the deviatoric stress versus axial strain plots for both the triaxial tests set A (Figure 9a) and the triaxial tests set B (Figure 9b) are shown. In Figure 10, the corresponding stress paths of the tests are put all together. If all the tests are considered, it should be detected a peak strength envelope that appears to be above the Critical State Line, with stress ratio $M = q_f/p'_f$ around 2 and corresponding to a peak friction angle of about 49°. This value is markedly higher than the repose angle of the material when cone-shaped as in Figure 1, which was around 40°, due to the more dense condition of the triaxial specimens, as discussed before.

Looking at the results of the direct shear tests (Figures 11 to 13), carried out on loose specimens to investigate the material strength at lower confining pressure, the strength envelope which refer to normal stresses beyond 10 kPa seems to be linear and a friction angle of 44°-47° can be deduced (Table 4), depending on the assumed interpolation line. At very low stresses, instead, the strength envelope appears to overcome the critical state resistance and a cohesion "intercept" of about 2-3 kPa, together with a friction angle of 56°, can be invoked (Table 4). It should be underlined, however, that the peak friction angles of soils are affected by the interpretation of the cohesion identified as intercept of the failure envelope. Indeed, the cohesion variability of both the lunar original soils and simulants is not negligible: 0.26-1.80 kPa for Lunar Regolith (Carrier et al. 1973), 0-2.0 kPa for BP-1 (Suescun-Florez et al. 2014), 3.9-14.4 kPa for JSC-1A according to Klosky et al. (2000) and 2.0-5.0 kPa for the same simulant according to Alshibli and Hasan (2009).

The dilative behaviour of DNA-1A at the lowest normal stresses suggests that the state of the specimens was probably on the left of the Critical State Line, CSL, in the specific volume - mean effective stress plane. This hypothesis is plausible given the high specific volumes characterizing the DNA-1A when uncompacted. Although the CSL has not been determined in the present work, on the basis of the yield stress range found by oedometer tests the transition between "dry of critical" and "wet of critical" soil behaviour should be expected in between the normal stress range investigated with shear box. In particular, the volumetric change behaviour under shearing (Figure 12) indicates that this transition occurs at normal stresses around 10 kPa. Further experimental data could corroborate this value, which is lower than that observed on other simulants with D_r about 60% (Ryu et al. 2018) and this difference can be justified by considering the lower relative density acquired by the shear box specimens of DNA-1A under self-weight compaction. Indeed, according to Ryu et al. (2018), FJS-1 and KLS-1 simulants showed slight dilation at low σ_v, becoming contractive at $\sigma_v > 50$ kPa, a threshold however higher than that found in the present study for DNA-1A when subjected to direct shear tests.

Summarizing, although more tests may be needed to refine the estimate, the strength parameters of DNA-1A (Table 4) seems to be consistent with those of the original lunar soils when in loose states. Self-weight compacted specimens with low relative density exhibit a non-linear strength envelope only at very low confining pressures, under which they dilate and overcome the critical state resistance. These mechanical

features should be taken into account in the calculation of soil-structure interaction, since a very low stresses range will be “operational” for geotechnical works under lunar gravity.

It should be underlined, however, that changes in particle surface energies with vacuum can result in soil mechanics tests of cohesive strength being different under vacuum than under usual laboratory conditions (Walton 2007). Therefore, mechanical tests aimed at determining the strength parameters and dilatancy angle of the loose lunar regolith should be performed at very low stress and under vacuum, also by developing new testing procedures.

Shear stiffness

The triaxial tests allow to measure the elastic moduli of the soil. In this case, the radial strain of the specimens has not been measured, therefore only the Young modulus E has been directly measured, although by assuming a Poisson ratio equal to 0.3 the shear modulus G has been deduced too. For most of the tests the shear stiffness refers to medium strains, whereas for two tests the stiffness values also refer to small strains, since they have been measured by local transducer, as described in the testing procedure. In Table 5 all the obtained Young modulus values are reported, together with the mean effective stress p’ and the strain level each measure refers to. The values obtained by external transducer have been calculated within the strain interval corresponding to the 10% of the deviatoric stress at failure. As expected, the values coming from local axial strain measurements are bigger than the corresponding values obtained by the external axial transducer: for the tests carried out at radial stress of about 40 kPa, the stiffnesses measured by external and by local transducer are about 6 MPa and 34 MPa respectively. The effect of the stress state on the material stiffness can also be detected from the table. Finally, the figure 14 reports the stiffness decay with axial strains for two tests: it seems that the plateau of elastic linearity has threshold at axial strain lower than 0.1%, probably at about 0.06-0.07%. Further experimental investigations are needed to deduce the dependency of this value on the relative density.

CONCLUSIONS AND FUTURE WORK

The geotechnical properties of the DNA-1A lunar regolith simulant have been shown and discussed, with specific reference to the soil when uncompacted. The grain size distribution, chemical composition, deformability and strength parameters have been found to be consistent with the original lunar soil and with other simulants. Due to its relatively low sorting, compared to other simulants, the DNA-1A could be preferred

when loose states must be achieved by uncompacted specimens. Moreover, from a chemical point of view, the amount of TiO2 makes the DNA-1A able to mimic low-Ti mare soil (Meurisse et al., 2017). For the investigated loose condition, the transition from dilative to contractive shear behaviour seems to occur at a normal confining stress of about 10 kPa. The elastic behaviour under shearing has been found, by using local strain gauge, to be linear up to almost 0.1 % axial strain.

The guidelines for building structures on the Moon should take into account the specific strength parameters of the regolith soils at very low pressures, which will characterize the soil-structure interaction at lunar gravity: in this case, it is required a specific interpretation of the failure criterion at very low confining stresses, taking into account the needed of serviceability assessment of geotechnical structures at ⅙ g gravity level. For the same reason, small strains are expected to be a crucial range for the design, therefore elastic moduli from local strain gauges should be preferred, since the medium strain stiffness has been found to be considerably lower. In this respect, the experimental results shown and discussed in this paper should be helpful.

The presented geotechnical characterization must be considered as preparatory to address future work, both numerical and experimental, aimed at investigating the soil-structure interaction for lunar geotechnical works under both static and dynamic conditions: in this respect, the Authors are implementing the geotechnical properties of DNA-1A in numerical simulations of the behaviour of physical models realized by employing this simulant.

REFERENCES

Alshibli K. A., Hasan A. (2009). *Strength properties of JSC-1A lunar regolith simulant.* J. Geotech. Geoenviron. Eng., 10.1061/(ASCE)GT.1943-5606.0000068, 673–679.

Atkinson J.H., Bransby P. L. (1978). *The mechanics of soils: an introduction to critical state soil mechanics*. McGraw-Hill Book Co, London; New York.

Cafaro F., Miticocchio E., Marzulli V. (2018). *Remarks on the reliability of physical modelling of lunar geotechnical structures.* Technical Note. Studia Geotechnica et Mechanica. Accepted for publication.

Carrier W.D. (1973). *Lunar soil grain size distribution, The Moon*, Vol. 6.

Carrier W.D. (2003). *Particle size distribution of lunar soil*. J. Geotech. Geoenviron. Eng., 10.1061/(ASCE)10900241(2003)129:10(956), 956–959.

Carrier W. D., Mitchell J. K., Mahmood A. (1973). *The nature of lunar soil.* J. Soil Mech. Found. Div., 99(10), 813–832.

Carrier, W. D., Olhoeft, G. R., and Mendell, W. (1991). Physical properties of the lunar surface. Lunar sourcebook, Cambridge University Press, New York, 475–594.

Cesaretti G., Dini E., De Kestelier X., Colla V., Pambaguian L. (2014). *Building components for an outpost on the lunar soil by means of a novel 3D printing technology*. Acta Astronautica, Vol. 93, pp. 430-450.

Costes N. C., Mitchell J. K. (1970). *Apollo 11: Soil mechanics investigation.* Proc., Apollo 11 Lunar Science Conf., Vol. 3, Lunar and Planetary Institute (LPI) and NASA Johnson Space Center (JSC), Houston, 2025–2044.

Cotecchia F., Chandler R.J. (2000). *A general framework for the mechanical behaviour of clays.* Géotechnique, 50, pp. 431-447.

Gromov V. V., Leonovich A. K., Lozhkin V. A., Rybakov A. V., Pavlov P.S., Dmitryev A. D., Shvarev V. V. (1972). *Results of investigations of the physical and mechanical properties of the lunar sample from Luna 16.* COSPAR Space Research XII, pp. 43–52. Akademie-Verlag, Berlin.

He C., Zeng X., Wilkinson A. (2013). *Geotechnical Properties of GRC-3 Lunar Simulant.* Journal of Aerospace Engineering, 26,3, 528-534.

Hight D. W., Bond A. J., Legge J. D. (1992). *Characterization of the Bothkennar clay: an overview.* Géotechnique, 42, pp. 303-347.

Hill E., Mellin M. J., Deane B., Liu Y., Taylor L. A. (2007). *Apollo sample 70051 and high-and low-Ti lunar soil simulants MLS-1A and JSC-1A: Implications for future lunar exploration.* J. Geophys. Res.:Planets, 112(E2), 1–11.

Kanamori H., Udagawa S., Yoshida T., Matsumoto S., Takagi K. (1998). *Properties of lunar soil simulant manufactured in Japan*. Proceedings of the 6th International Conference and Exposition on Engineering Construction, and Operations in Space. ASCE, Albuquerque, NM, USA, pp. 462-468.

Klosky J. L., Sture S., Ko H. Y., Barnes F. (2000). *Geotechnical behaviour of JSC-1 lunar soil simulant*. J. Aerosp. Eng., 10.1061/ (ASCE)0893-1321(2000)13:4(133), 133–138.

Leonovich A.K., Gromov V.V., Dmitriyev A.D., Penetrigov V.N., Semenov P.S., Shvarev V.V. (1974) *The main peculiarities of the processes of the deformation and destruction of lunar soil.* In The Soviet American Conference on Cosmochemistry of the Moon and Planets, pp. 735–743. NASA SP-370 (1977); also available in NASA Technical Translation F-16034 (1974).

Leonovich A. K., Gromov V. V., Semyonov P. S., Penetrigov V. N., Shvaryov V.V.(1975) *Luna 16 and 20 investigations of the physical and mechanical properties of lunar soil.* In COSPAR Space Research XV, pp. 607–616. Akademie-Verlag, Berlin.

Liu Y., Park J., Schnare D., Hill E., Taylor L.A. (2008). *Characterization of lunar dust for toxicological studies. II: Texture and shape characteristics.* J. Aerosp. Eng., 10.1061/(ASCE)0893-1321(2008) 21:4(272), 272–279.

Meurisse A., Beltzung J. C., Kolbe M., Cowley A., Sperl M. (2017). *Influence of Mineral Composition on Sintering Lunar Regolith.* J. Aerosp. Eng., 2017, 30(4): 04017014.

Markandeya Raju P., Pranathi S. (2012). *Lunarcrete -A Review.* Proceedings of AARCV 2012 - International Conference on Advances in Architecture and Civil Engineering, 21st – 23rd June 2012 Paper ID AR84AS, Vol.2, pp. 886-891.

McKay D., Carter J., Boles W., Allen C., Allton J. (1994). *JSC-1: A new lunar soil simulant.* Engineering, Construction, and Operations in Space IV, pp. 857–866.

Omura T., Kiuchi M., Guttler C., Nakamura A.M. (2016). *Centrifugal Experiments with Simulated Regolith: Effects of Gravity, Size Distribution, and Particle Shape on Porosity*. Transactions of the Japan Society for Aeronautical and Space Sciences, Aerospace Technology Japan. 14. Pk_17-Pk_21. 10.2322/tastj.14.Pk_17.

Perkins S.W., Madson C.R. (1996). *Mechanical and load-settlement characteristics of two lunar soil simulants.* J. Aerosp. Eng., 10.1061/(ASCE)0893-1321(1996)9:1(1), 1–9.

Pitcher C., Kömle N., Leibniz O., Morales-Calderon O., Gao Y., Richter L. (2016). *Investigation of the properties of icy lunar polar regolith simulants.* Advances in Space Research, Volume 57, Issue 5, 2016, Pages 1197-1208, ISSN 0273-1177.

Rickman D., McLemore C., Fikes J. (2007). *Characterization summary of jsc-1a bulk lunar mare regolith simulant.* National Aeronautics and Space Administration, Washington, DC.

Ryu B.H., Wang C.C., Chang I. (2018). *Development and Geotechnical Engineering Properties of KLS-1 Lunar Simulant*. Journal of Aerospace Engineering, 31, 04017083.

Schofield A. N., Wroth C. P. (1968). *Critical State Soil Mechanics.* McGraw-Hill, p. 310, ISBN 978-0641940484.

Schrader C.M., Rickman D., McLemore C., Fikes J., Stoeser D., Wilson S., Butcher A., Botha P.W.S.K. (2008). *Extant and Extinct Lunar Regolith Simulants: Modal Analyses of NU-LHT-1m and -2m, JSC-1, JSC-1A and -1AF, and FJS-1, and MLS-1*. Planetary Mining and Science Symp., Montreal.

Schrader C., Rickman D., McLemore C., Fikes J. (2010). *Lunar Regolith Simulant User's Guide.* NASA/TM-2010-216446, NASA Centre for Aerospace Information, Hanover, USA.

Stoeser D. B., Rickman D. L., Wilson S. (2010). *Preliminary geotechnical findings on the BP-1 simulant.* NASA/TM—2010-216444, NASA, Marshall Space Flight Center, AL.

Suescun-Florez E., Roslyakov S., Iskander M., Baamer M. (2014). *Geotechnical Properties of BP-1 Lunar Regolith Simulant.* Journal of Aerospace Engineering. 28. 04014124. 10.1061/(ASCE)AS.1943-5525.0000462.

Walton O. R. (2007). *Adhesion of Lunar Dust.* NASA/CR—2007-214685.

Willman B., Boles W., McKay D., Allen C. (1995). *Properties of lunar soil simulant JSC-1*. J. Aerosp. Eng. 8, 77–87.

Wils L., Van Impe P.O., Haegeman W. (2015). *One-dimensional compression of a crushable sand in dry and wet conditions.* Geomechanics from Micro to Macro – Soga et al. (Eds) pp. 1403-1408.

Wood D. M. (1990). *Soil Behaviour and Critical State Soil Mechanics.* 10.1017/CBO9781139878272.

FIGURE CAPTIONS

Figure 1 - Cone-shaped lunar simulant DNA-1A deposit: plan view (Image by authors)

Figure 2: a) Particle-size distribution of DNA-1A lunar simulant; b) Comparison with lunar regolith and other simulants

Figure 3 - Chemical composition of DNA-1A lunar simulant

Figure 4 - SEM images at different magnification (75x, 400x, 750x, 850x, 1100x, 1200x): a) general view of DNA-1A simulant (75x); b) clast with vesicles and fragments of juvenile material (400x); c) clast with vesicles of irregular shape generated by the presence of magma (1100x); d) detail of a vesicle (1200x); e-f) fragments of juvenile material rich in crystal and minerals (750x; 850x)

Figure 5 - High pressure oedometer apparatus, with three loading arms (Image by authors)

Figure 6 - Triaxial specimen preparation with thick (a) and thin (b) membrane and local axial transducer (c) (Images by authors)

Figure 7- Oedometer compression curves for MP5, MPW. HP5,HP15 tests

Figure 8 – Void ratio versus time plot for the last loading step of HP15 test

Figure 9 - Deviatoric stress versus axial strain plots for set A (a) and set B (b) triaxial tests

Figure 10 -Stress paths followed by all the specimens subjected to triaxial compression

Figure 11 - Tangential force versus horizontal displacement during direct shear tests

Figure 12 - Vertical versus horizontal displacements during direct shear tests

Figure 13 - Shear stress versus normal stress at failure

Figure 14 - Stiffness decay with strain, measured by local strain gauge during the tests A-TRX-40kPa (a) and A-TRX-20kPa (b)

Table 1 - Chemical composition of DNA-1 (Cesaretti et al. 2014), JSC-1A (Rickman et al. 2007), Lunar Soil 14163 (mean of the Apollo missions; Cesaretti et al. 2014) and DNA-1A.

Oxide	JSC-1A (wt. %)	DNA-1 (wt. %)	DNA-1A (wt. %)	Lunar Soil 14163 (wt. %)
SiO_2	46.67	41.90	51.97	47.30
TiO_2	1.71	1.31	0.85	1.60
Al_2O_3	15.79	16.02	18.02	17.80
Fe_2O_3	3.41	14.60	7.07	0.00
FeO	7.57	/	/	10.50
MgO	9.39	6.34	2.70	9.60
CaO	9.90	12.90	7.40	11.4
Na_2O	2.83	2.66	4.81	0.70
K_2O	0.78	2.53	4.63	0.60
MnO	0.19	0.21	0.14	0.10
P_2O_5	0.66	0.34	0.41	0.00
LOI	0.00	0.00	2.00	0.00

Table 2 - Minimum and maximum soil densities and void ratios of DNA-1A, together with ranges for Lunar Soil 14163 (Carrier et al. 1973; Carrier 1973).

	DNA-1A	**Lunar Soil 14163**
ρ_{min} **(g/cm^3)**	0.98	0.87-1.36
ρ_{max} **(g/cm^3)**	1.57	1.51-1.93
e_{min}	0.72	/
e_{max}	1.76	/

Table 3 – Compressibility parameters of lunar simulant DNA-1A

	Recompression index	**Compression index**	**Swelling index**
MP5	0.061-0.083	0.224	0.013
MPW	0.048-0.067	0.225	0.010
HP5	0.088-0.104	0.333	/
HP15	0.092	0.325	/

Table 4 - Strength parameters of loose DNA-1A for different pressure ranges, as measured with direct shear tests.

Strength parameters	**Low pressure range [< 10 kPa]**	**Medium pressure range [> 10 kPa]**
c' (kPa)	2-3	0
ϕ' (°)	56	44-47

Table 5 - Young modulus values of DNA-1A for different confining pressures and strain intervals of measurement.

E (kPa)	**p' (KPa)**	**Axial strain interval (%)**
42065	158	0.17
19814	102	0.25
9537	102	0.56
7828	67	0.53
7183	60	0.27
6057	43	0.20
34129(*)	41	6.2094E-03
33077(*)	21	6.01343E-03

*with local strain gauge

Figure 1

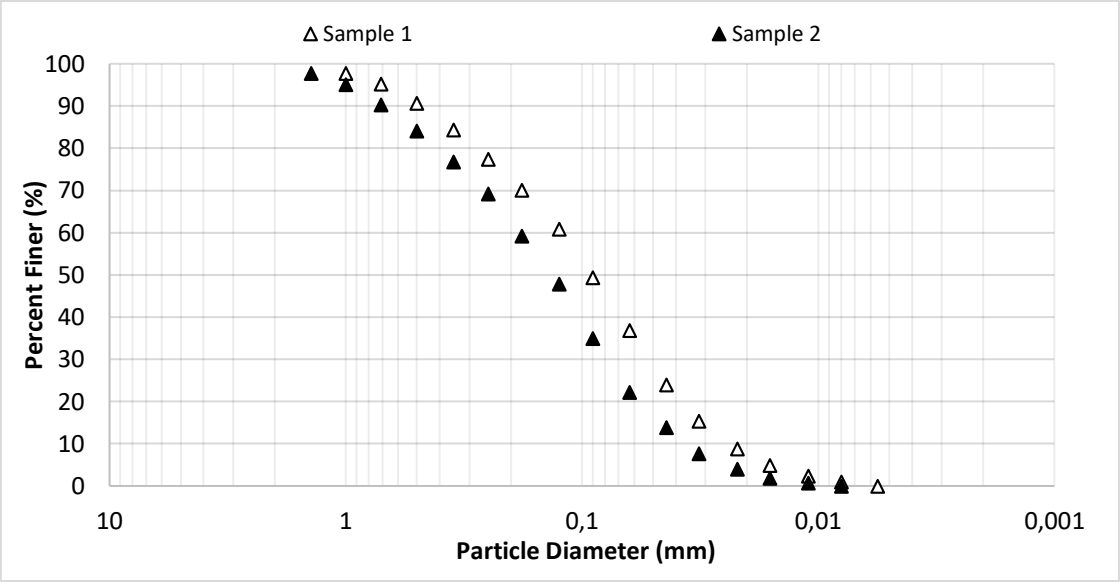

Figure 2a

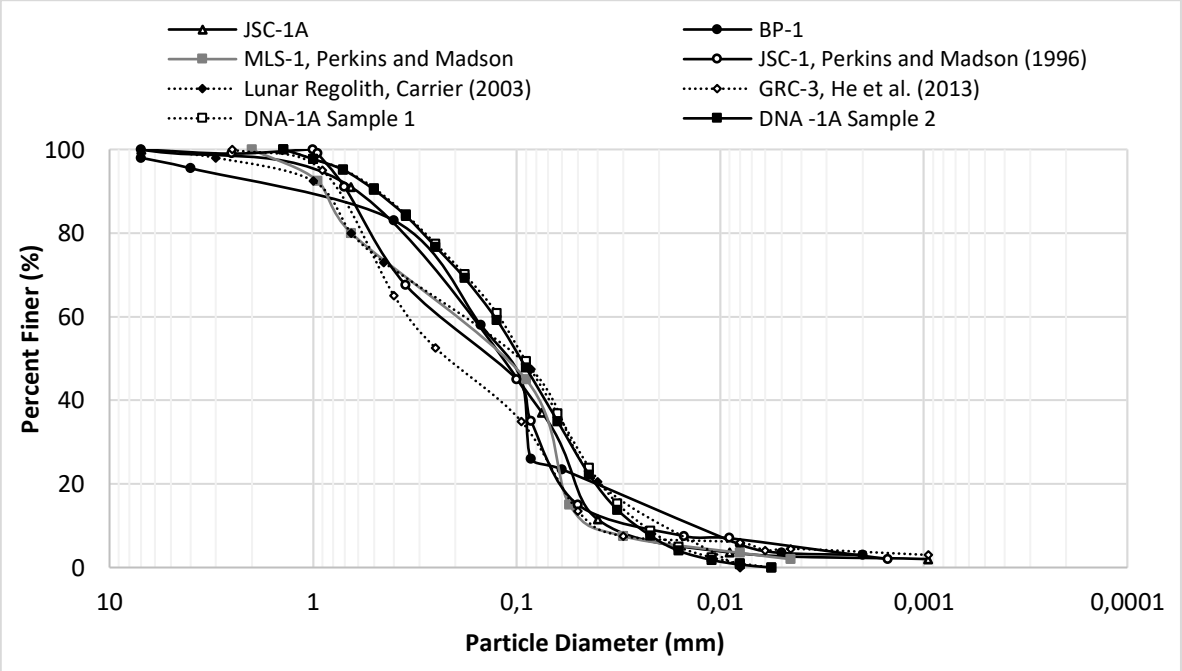

Figure 2b

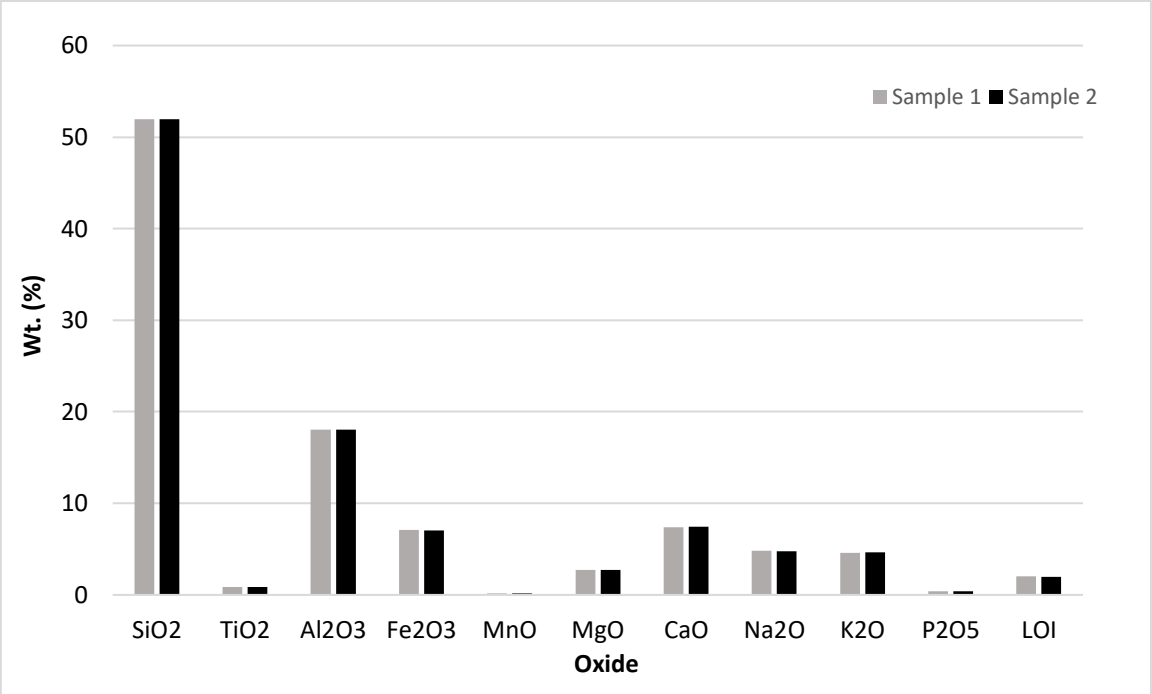
60
50
40
30
20
10
0
Wt. (%)
Sample 1
Sample 2
SiO2
TiO2
Al2O3
Fe2O3
MnO
MgO
CaO
Na2O
K2O
P2O5
LOI
Oxide

Figure 3

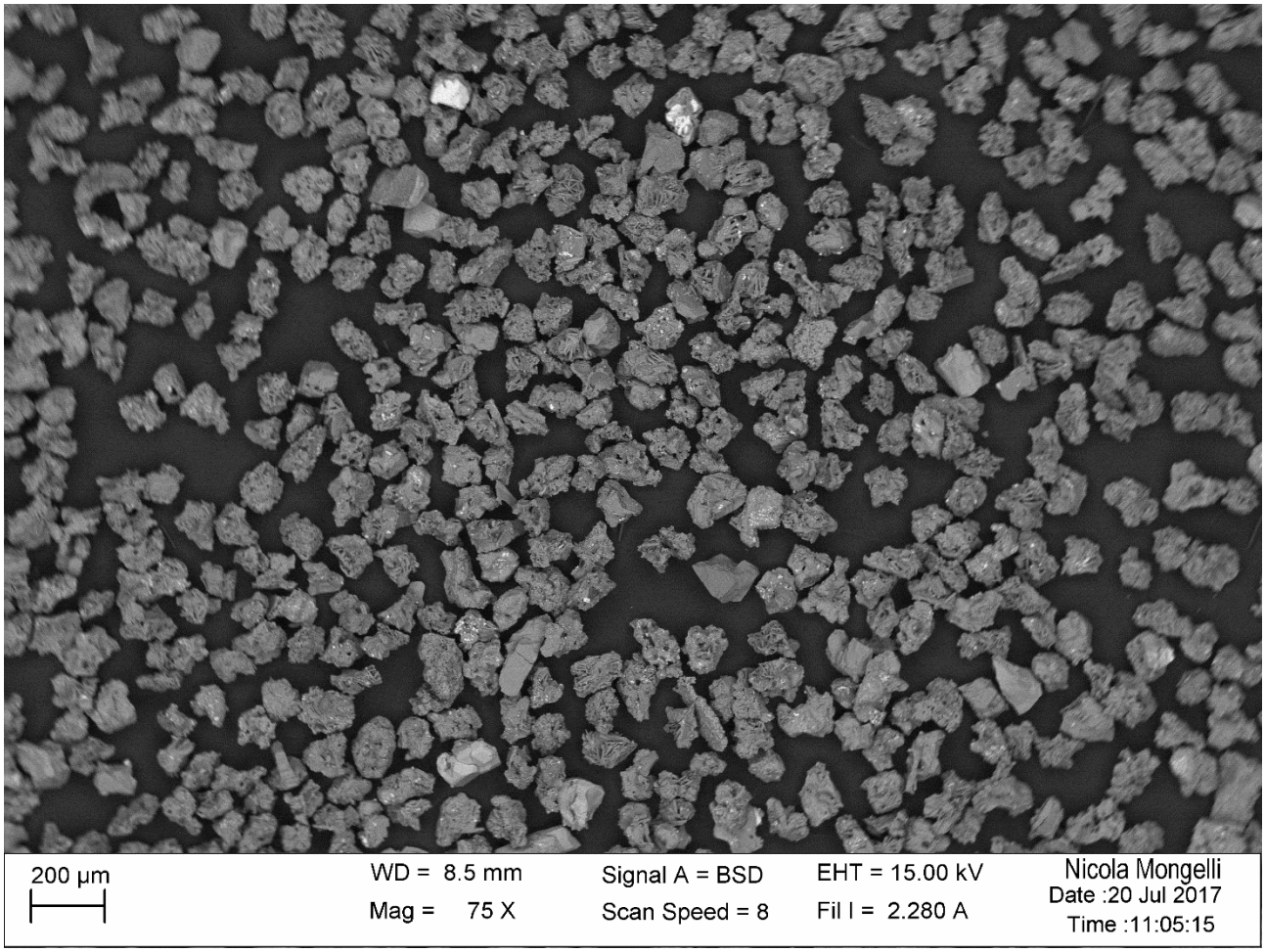
200 µm
WD = 8.5 mm
Mag = 75 X
Signal A = BSD
Scan Speed = 8
EHT = 15.00 kV
Fil I = 2.280 A
Nicola Mongelli
Date :20 Jul 2017
Time :11:05:15

Figure 4a

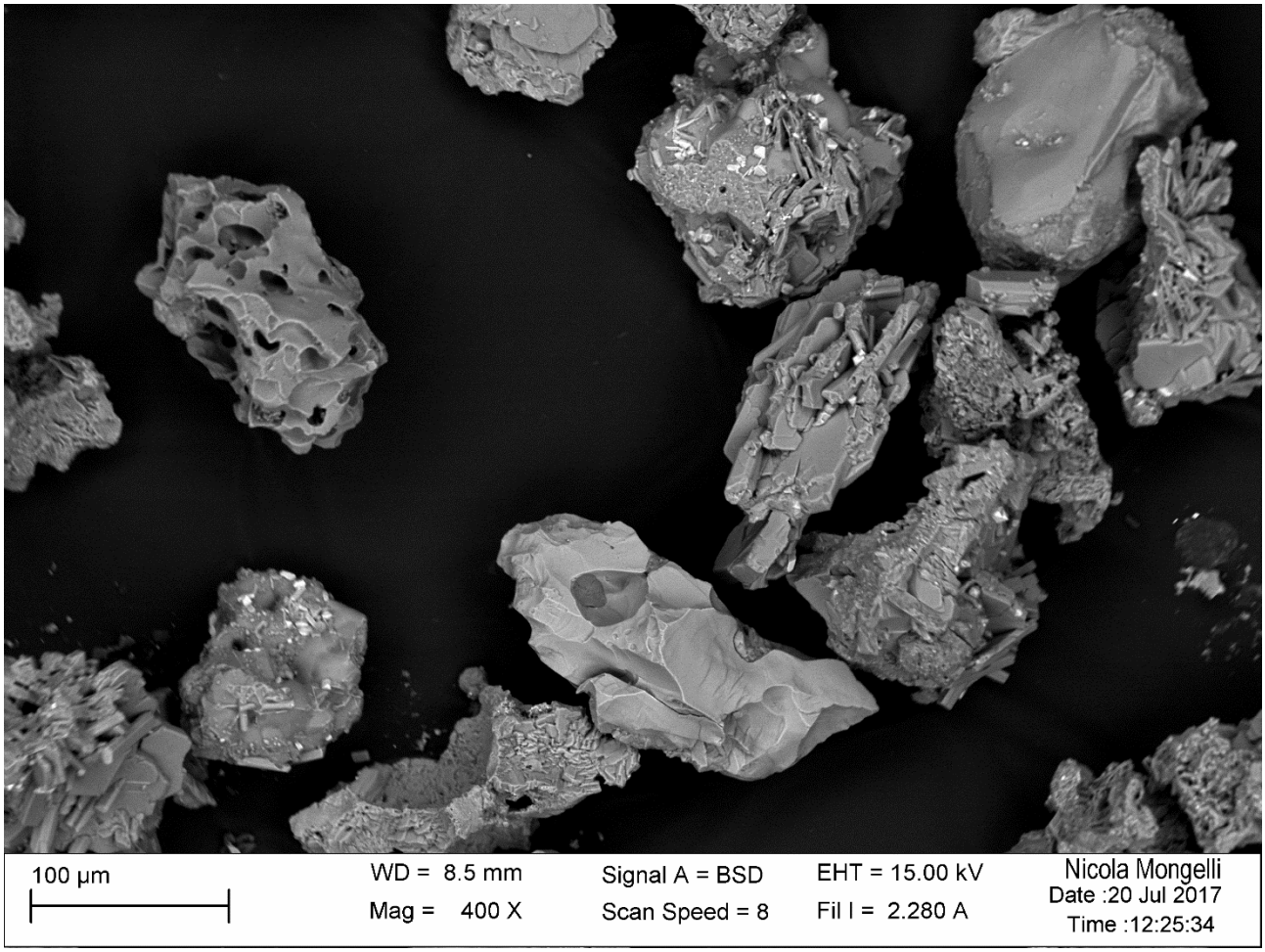
100 µm
WD = 8.5 mm
Mag = 400 X
Signal A = BSD
Scan Speed = 8
EHT = 15.00 kV
Fil I = 2.280 A
Nicola Mongelli
Date :20 Jul 2017
Time :12:25:34

Figure 4b

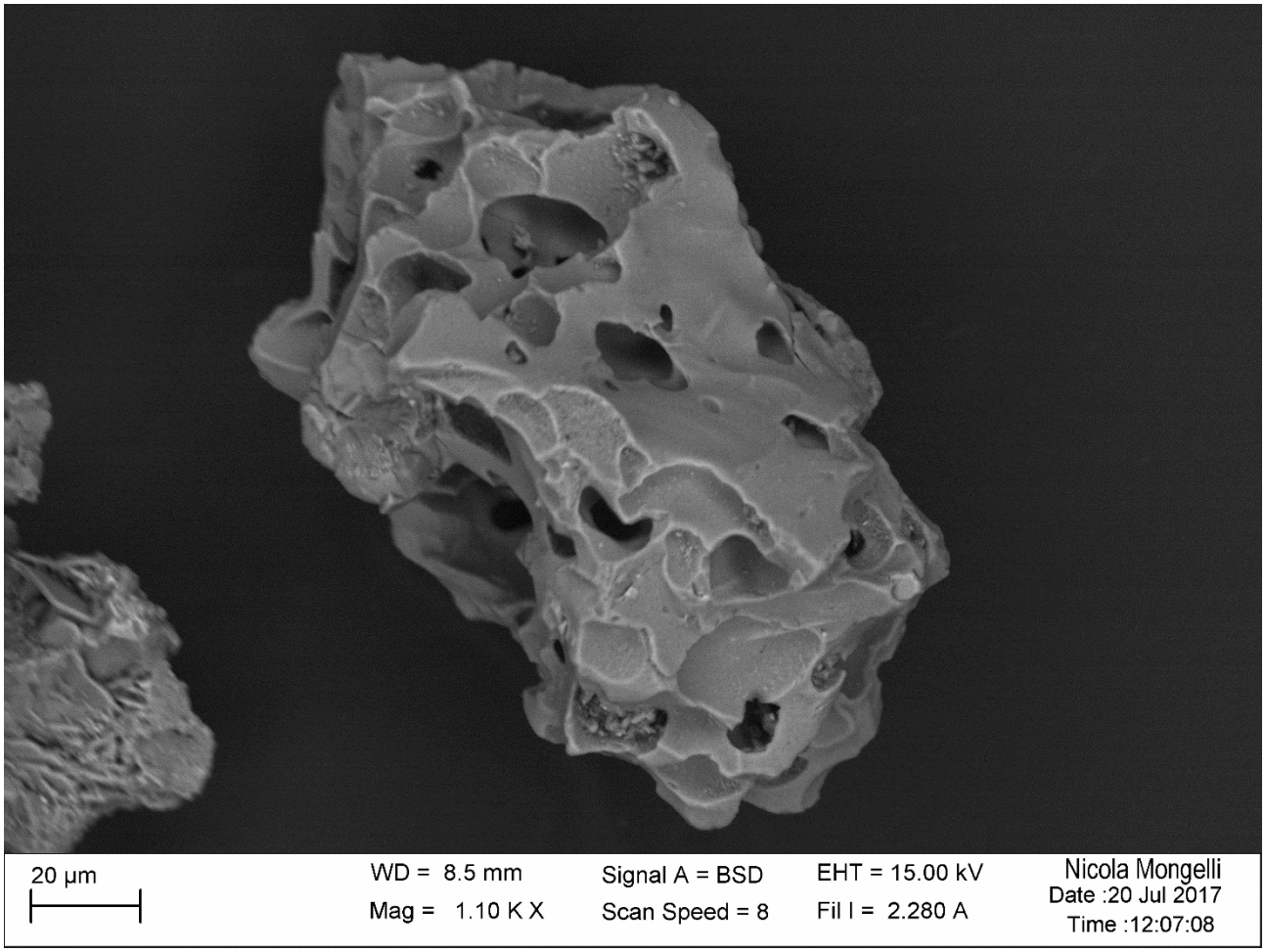
20 µm
WD = 8.5 mm
Mag = 1.10 K X
Signal A = BSD
Scan Speed = 8
EHT = 15.00 kV
Fil I = 2.280 A
Nicola Mongelli
Date :20 Jul 2017
Time :12:07:08

Figure 4c

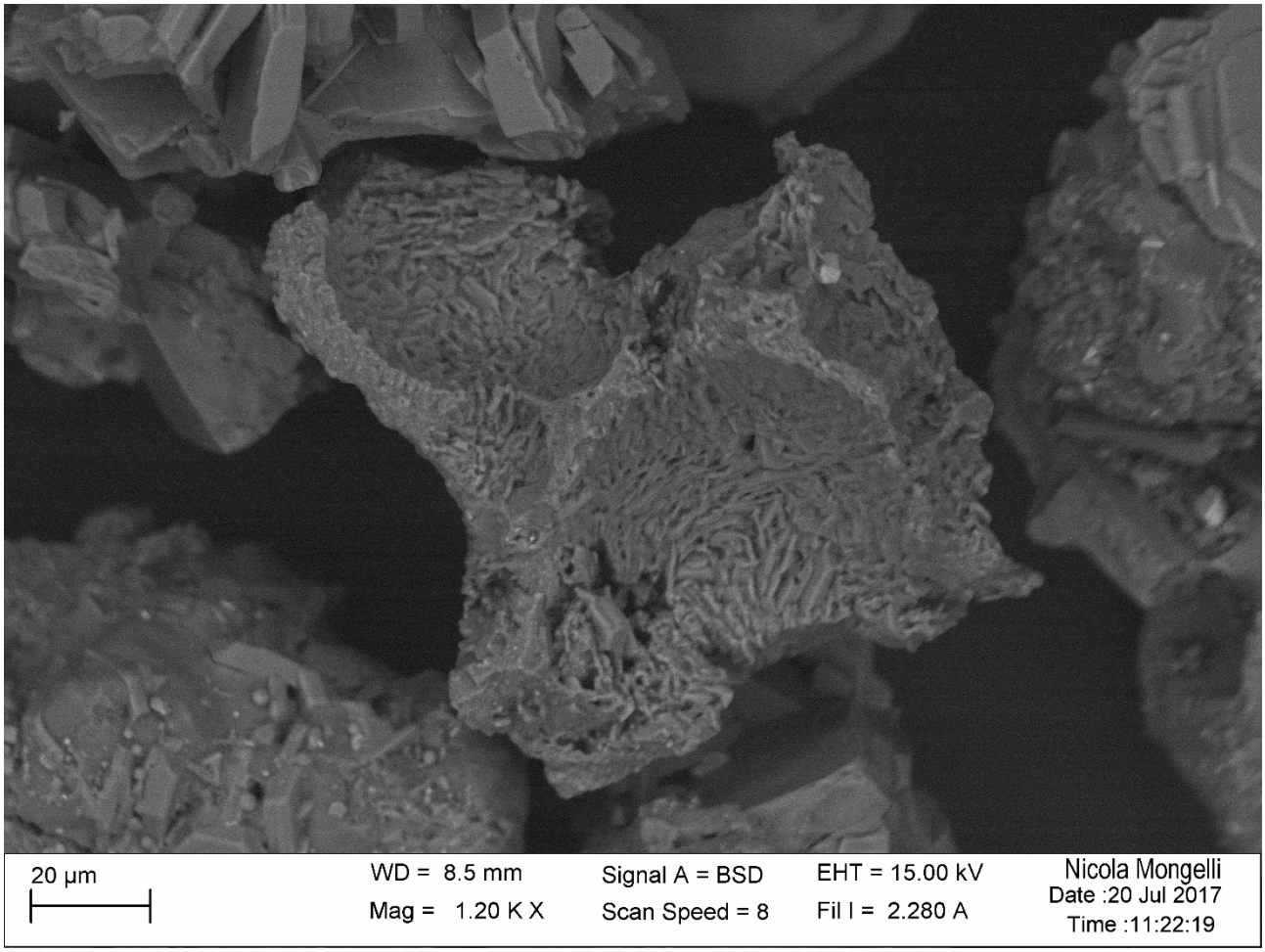
20 µm
WD = 8.5 mm
Mag = 1.20 K X
Signal A = BSD
Scan Speed = 8
EHT = 15.00 kV
Fil I = 2.280 A
Nicola Mongelli
Date :20 Jul 2017
Time :11:22:19

Figure 4d

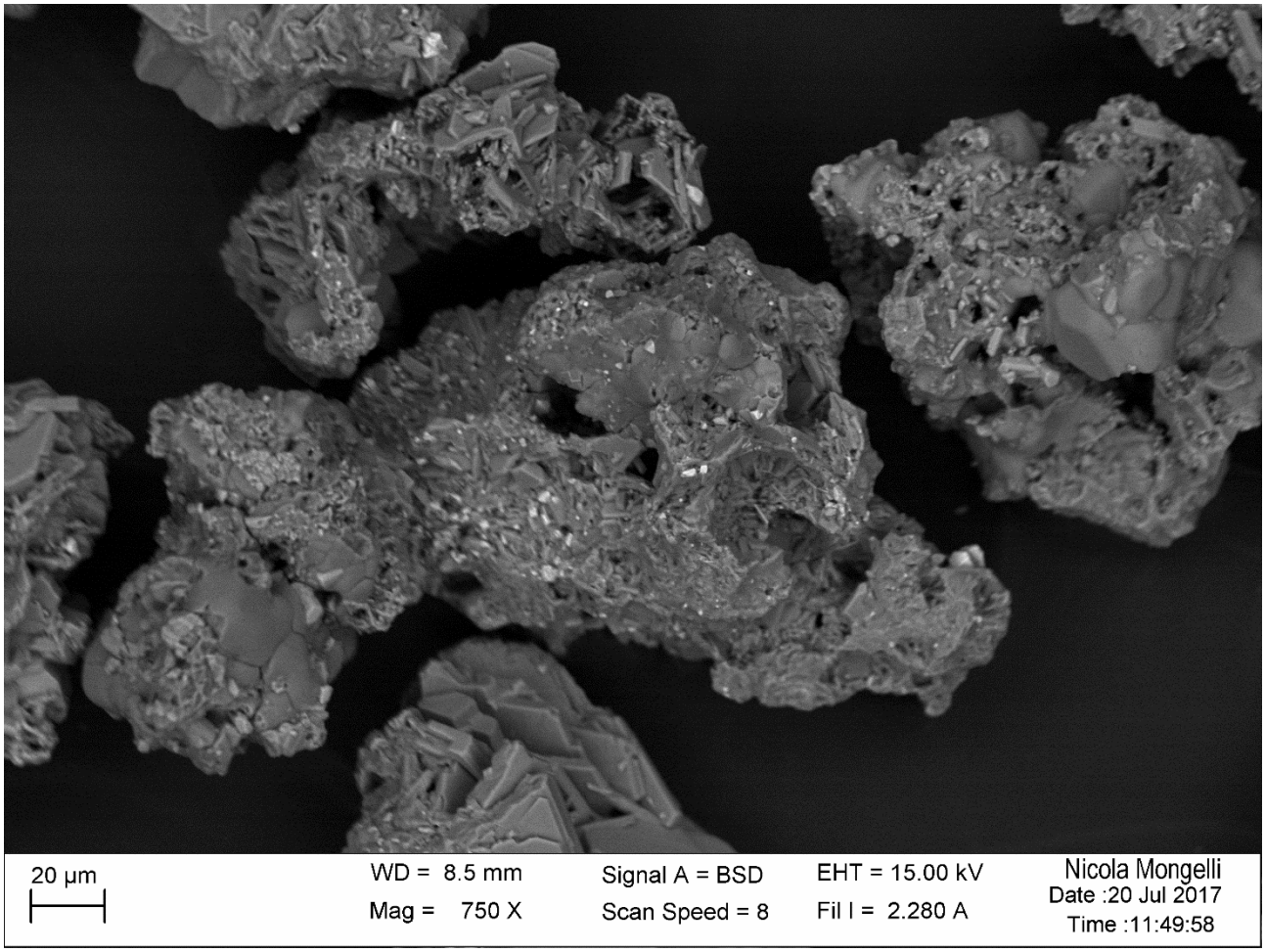
20 µm
WD = 8.5 mm
Mag = 750 X
Signal A = BSD
Scan Speed = 8
EHT = 15.00 kV
Fil I = 2.280 A
Nicola Mongelli
Date :20 Jul 2017
Time :11:49:58

Figure 4e

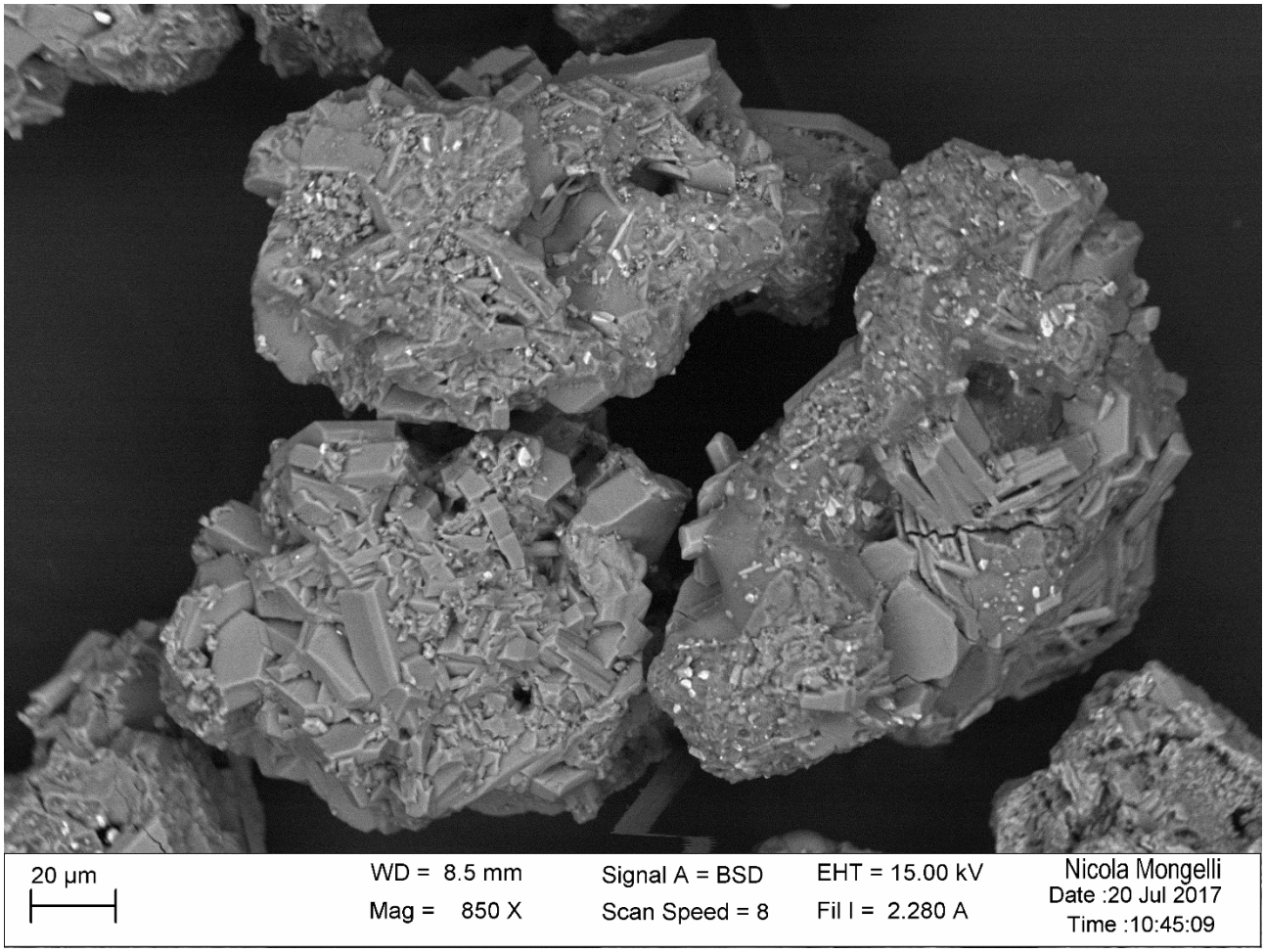
20 µm
WD = 8.5 mm
Mag = 850 X
Signal A = BSD
Scan Speed = 8
EHT = 15.00 kV
Fil I = 2.280 A
Nicola Mongelli
Date :20 Jul 2017
Time :10:45:09

Figure 4f

Figure 5



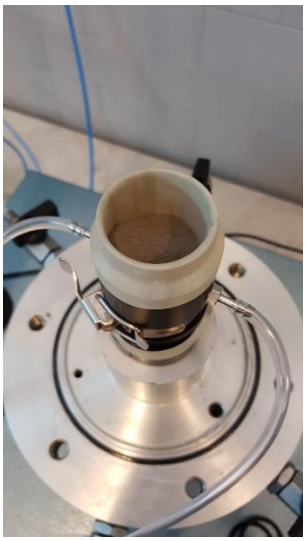

Figure 6a- 6b-6c

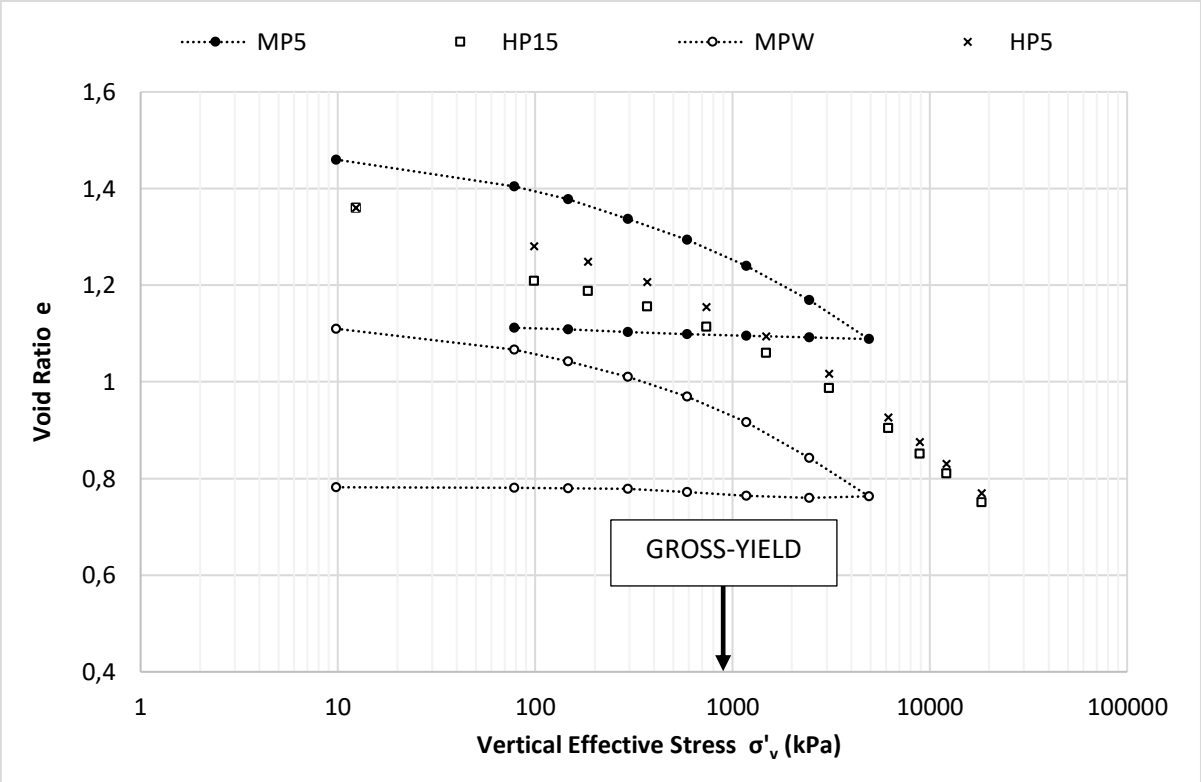
MP5
HP15
MPW
HP5
1,6
1,4
1,2
1
0,8
0,6
0,4
Void Ratio e
GROSS-YIELD
1
10
100
1000
10000
100000
Vertical Effective Stress σ'v (kPa)

Figure 7

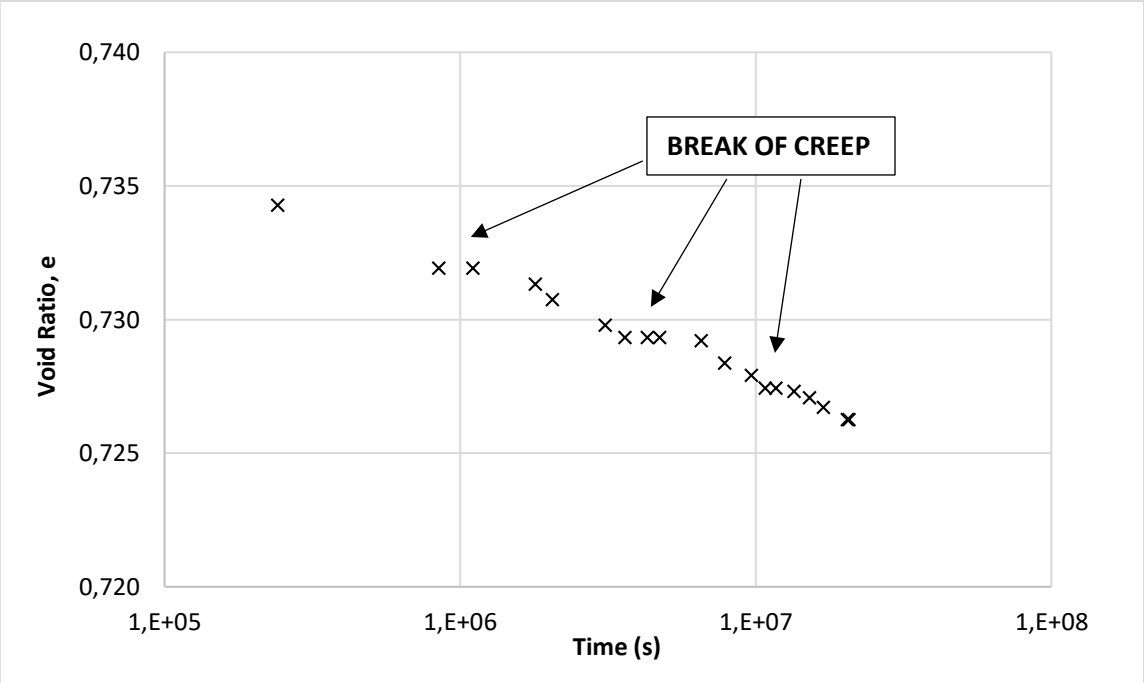
0,740
0,735
0,730
0,725
0,720
Void Ratio, e
BREAK OF CREEP
1,E+05
1,E+06
1,E+07
1,E+08
Time (s)

Figure 8

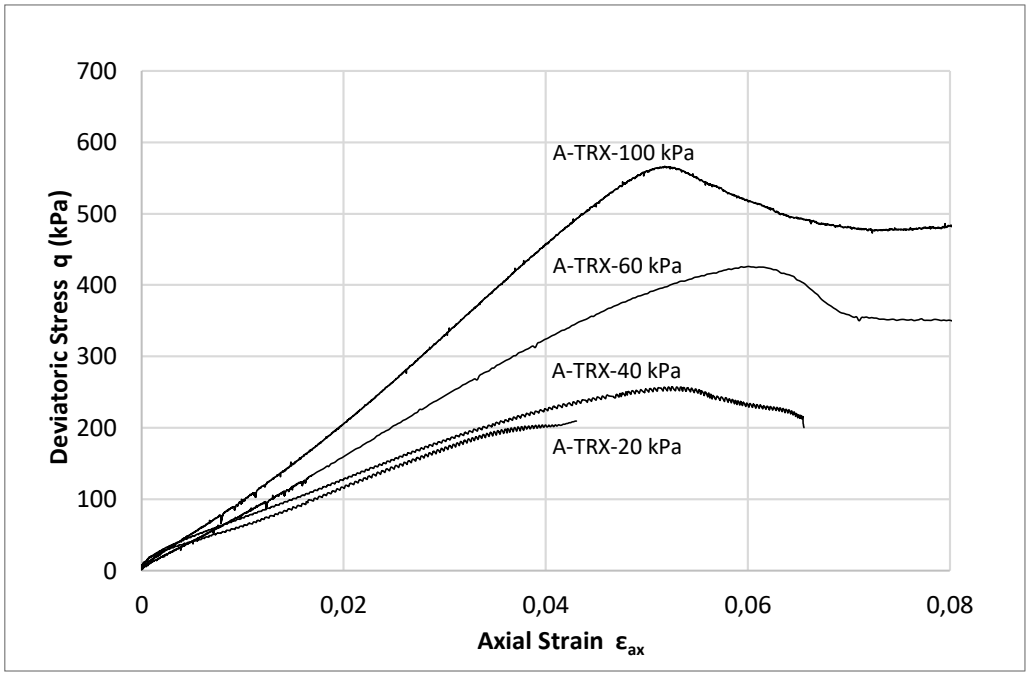

Figure 9a

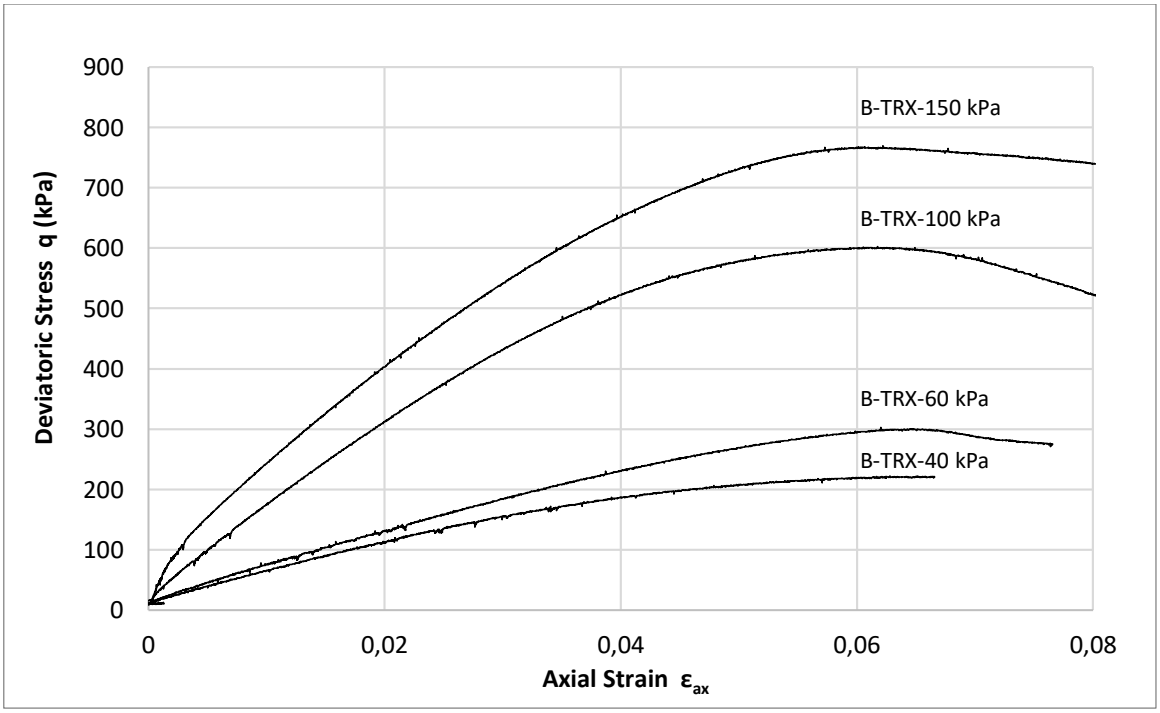

Figure 9b

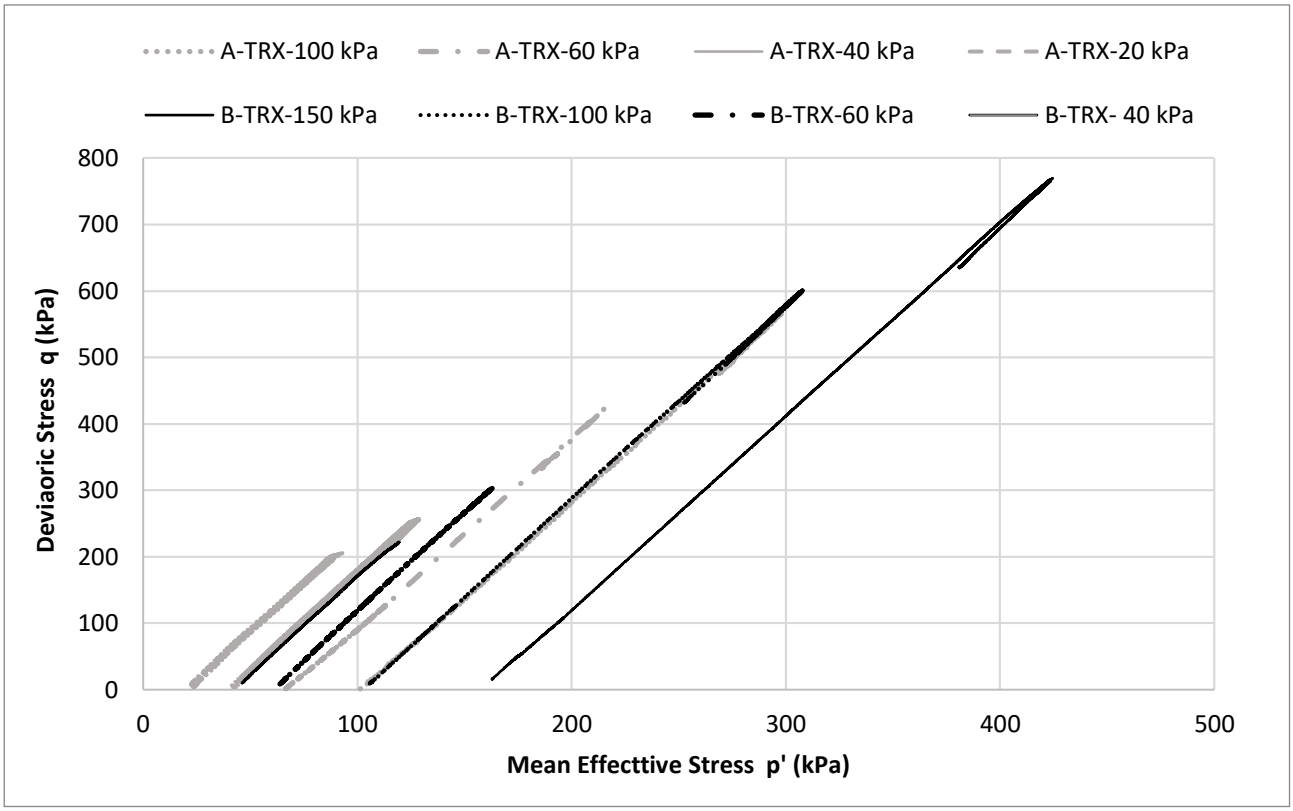
A-TRX-100 kPa
A-TRX-60 kPa
A-TRX-40 kPa
A-TRX-20 kPa
B-TRX-150 kPa
B-TRX-100 kPa
B-TRX-60 kPa
B-TRX- 40 kPa
Deviaoric Stress q (kPa)
0
100
200
300
400
500
600
700
800
0
100
200
300
400
500
Mean Effecttive Stress p' (kPa)

Figure 10

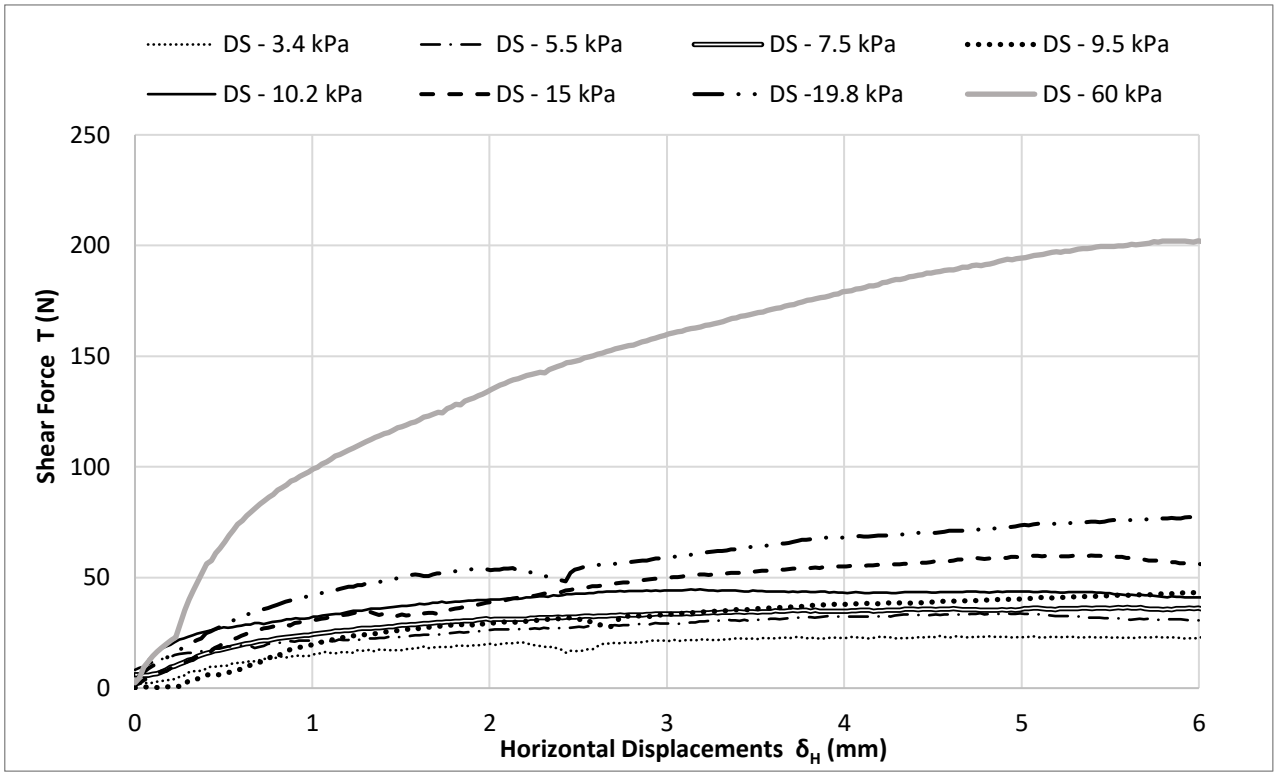
DS - 3.4 kPa
DS - 5.5 kPa
DS - 7.5 kPa
DS - 9.5 kPa
DS - 10.2 kPa
DS - 15 kPa
DS -19.8 kPa
DS - 60 kPa
Shear Force T (N)
250
200
150
100
50
0
0
1
2
3
4
5
6
Horizontal Displacements δH (mm)

Figure 11

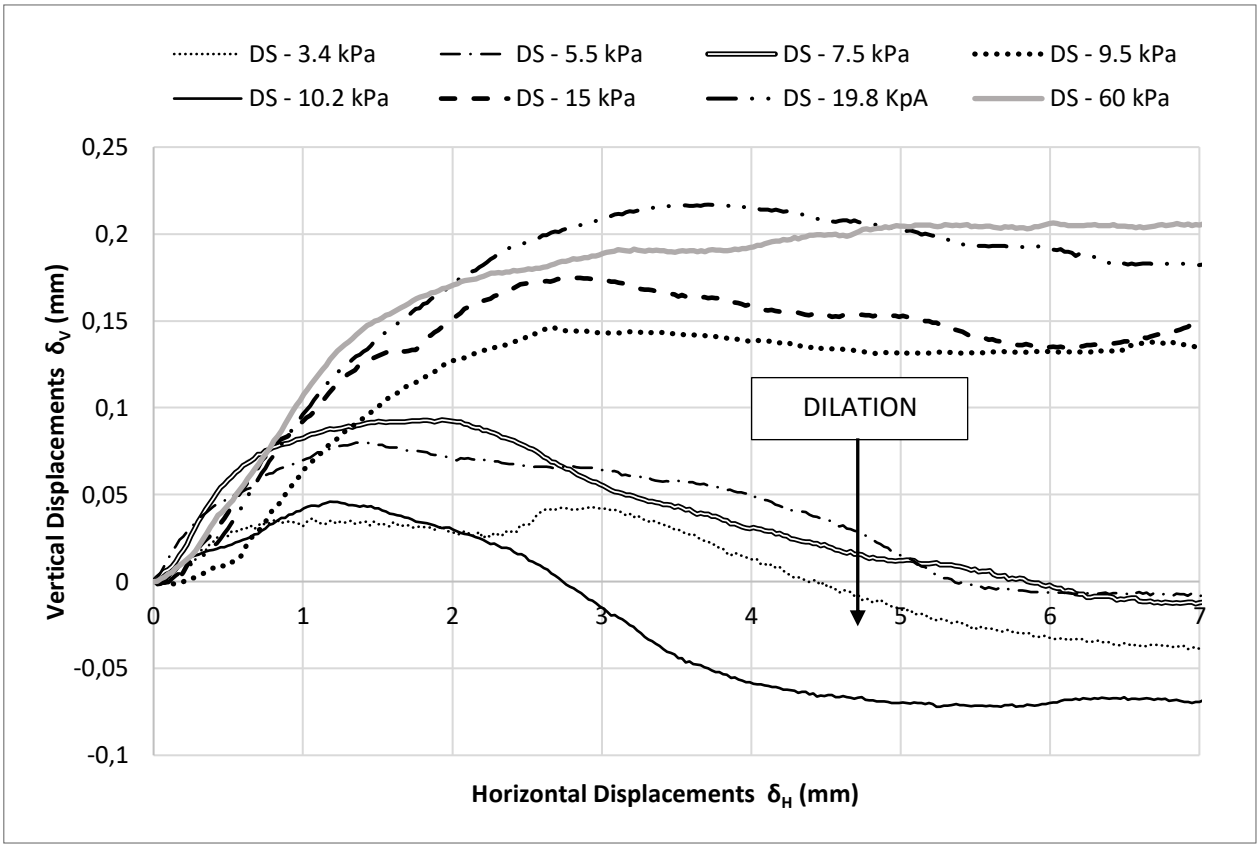
DS - 3.4 kPa
DS - 5.5 kPa
DS - 7.5 kPa
DS - 9.5 kPa
DS - 10.2 kPa
DS - 15 kPa
DS - 19.8 KpA
DS - 60 kPa
0,25
0,2
0,15
0,1
0,05
0
-0,05
-0,1
Vertical Displacements δ_V (mm)
DILATION
0
1
2
3
4
5
6
7
Horizontal Displacements δ_H (mm)

Figure 12

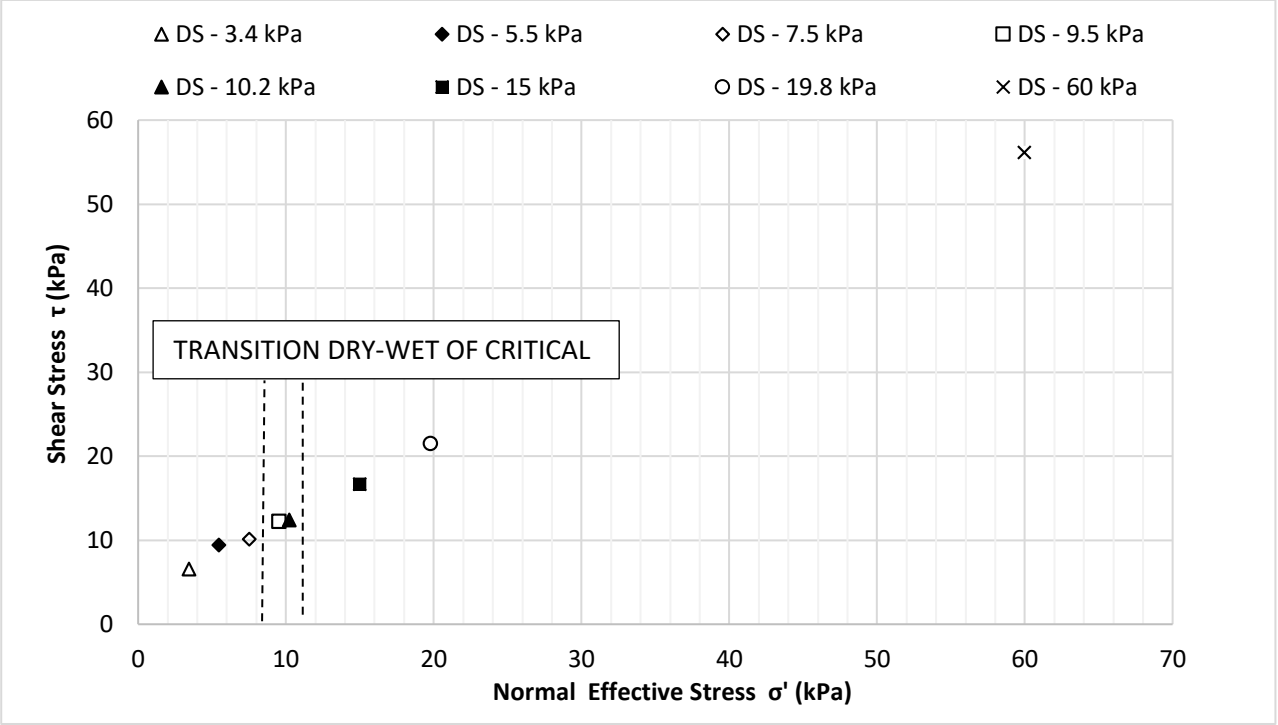
△ DS - 3.4 kPa
◆ DS - 5.5 kPa
◇ DS - 7.5 kPa
□ DS - 9.5 kPa
▲ DS - 10.2 kPa
■ DS - 15 kPa
○ DS - 19.8 kPa
× DS - 60 kPa
TRANSITION DRY-WET OF CRITICAL
Shear Stress τ (kPa)
Normal Effective Stress σ' (kPa)
0
10
20
30
40
50
60
70

Figure 13

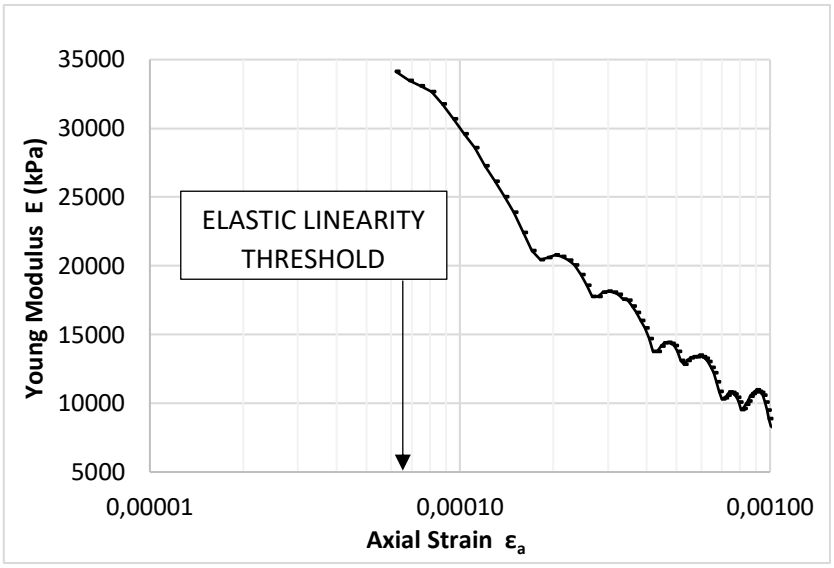

Figure 14a

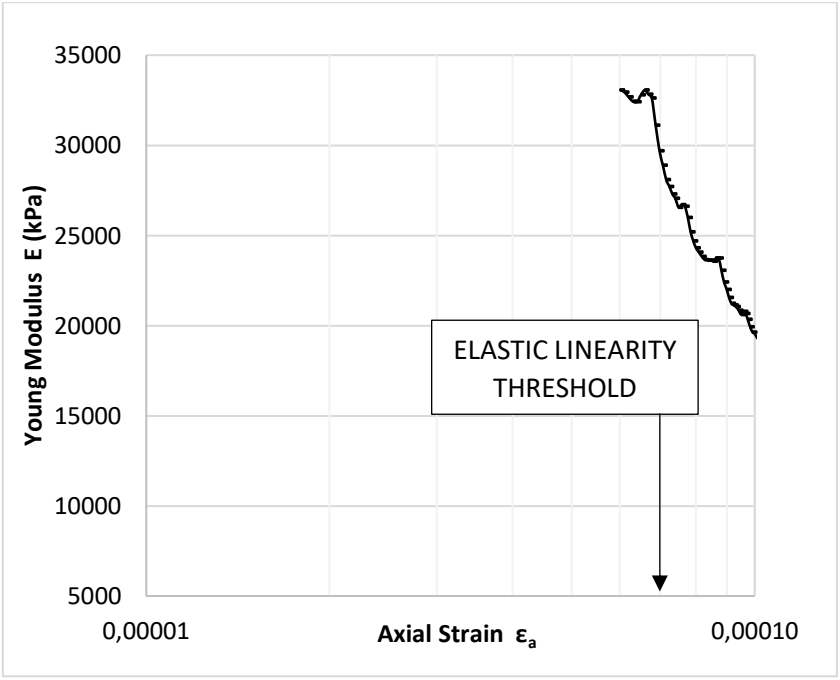

Figure 14b